JOURNAL OF COMPUTATIONAL PHYSICS 111, 165–182 (1994)

# Numerical Simulation of Stratified Coating Flow by a Variational Method

D. BERGHEZAN AND F. DUPRET

*Unité de Mécanique Appliquée, Université Catholique de Louvain, 4 av. G. Lemaître, 1348 Louvain-la-Neuve, Belgium*

Received June 29, 1991; revised December 23, 1992

We present a method for calculating the two-dimensional steady state flow of stratified Newtonian liquids. Lagrange multipliers are used to impose the free surface conditions. When surface tension is not vanishing, contact angles are easily introduced. Inlet and outlet free sections are treated by means of a technique which allows us to calculate layer thicknesses as part of the result. Parametric studies are thereby facilitated. The solution procedure is derived from a variational approach. At each iteration, a linear system is obtained by linearizing the weak form of the problem. A finite element discretization is carried out on this continuous system. The mesh is adapted to the successive configurations of the free boundaries. Ill-shaped elements are corrected by exerting artificial forces on the mesh vertices. The global iterative scheme exhibits a quasi-quadratic convergence. The outflow from a slot and the curtain coating flow are analysed and illustrate the power of the method. 

## 1. INTRODUCTION

The film coating process consists in simultaneously spreading several liquid layers onto a moving plastic support. As each liquid has specific properties, a very precise uniformity of the layers is required. Improving the technique has been a constant objective in the photographic industry and has led to developing several procedures, among which the slide coating and the curtain coating processes should be retained. A discussion of the advantages and difficulties of curtain coating may be found in Pulkrabek and Wabrek [1].

Mathematical analysis is of course essential to understand the physics of the phenomena involved (viscosity, surface tension, inertial effects). A general theory of film coating is given in Deryagin and Levi [2]. However, this approach has strong limitations because the problem is highly non-linear. Hence, as experiments are long and very expensive, using the predictive capacity of modern computers has become more and more widespread for the last decade. Numerical simulation of film coating was initiated by Saito and Scriven [3], Kistler and Scriven [4], and Kistler [5], whose contributions should be stressed. In this paper, we focus on calculating the flow in critical regions, such as the curtain flow or the outflow from a slot—where a supplementary layer is injected under a stratified flow. These calculations provide important information concerning the presence of recirculations, the configuration of the interfaces, and the location of their origin on the wall. An additional objective would be to predict the flow stability. This problem, which is addressed in Christodoulou and Scriven [6], is not examined here.

We present an original method for calculating the two-dimensional steady state isothermal flow of stratified Newtonian liquids. This method is an extension of the work of Dupret [7–9] and is devoted to solving free boundary problems, with or without surface tension, using the Galerkin finite element technique in the velocity–pressure formulation. A particular feature lies in introducing Lagrange multipliers (following Babuška [10]) for imposing the kinematic condition on the free surfaces. The normal stress condition is also imposed in a weak sense, and, when surface tension is not vanishing, integration by parts of this equation is carried out over the free boundaries in a suitable manner, which is similar, but differs from the method of Ruschak [11]. Contact angles are thereby easily imposed at the ends of these lines. Moreover, inlet and outlet free sections are treated by means of a particular technique—also based on the use of Lagrange multipliers—which does not require us to impose the layer thicknesses, but to calculate the latter as part of the result. Parametric studies are facilitated, since solutions may be obtained sequentially by using each successive result as an initial value for a new calculation.

The solution procedure is derived from a variational approach. At each iteration, the linear system to be solved is obtained by linearizing the weak form of the problem. Discretization is carried out on this continuous system. The same technique was used in Dupret [7, 9] and in Kruyt *et al.* [12]. After solution of the linear system, each iteration is followed by a correction step. The mesh is moved in order to be adapted to the new configuration of the free



0021-9991/94 $6.00

boundaries, and the nodal values of the unknowns are corrected according to mesh deformation. In order to obtain well-behaved elements, a particular algorithm has been developed, which consists in exerting appropriate "pseudo-forces" at the vertices of the elements, in such a manner that overly acute or obtuse angles tend to be corrected. Mesh correction is decoupled from the solution of the linear system. The global iterative scheme exhibits a quasi-quadratic convergence. Several examples are analysed and illustrate the power of the method.

## 2. DESCRIPTION OF THE PROBLEM

### 2.1. Strong Formulation

Consider in Fig. 1 a schematic description of (a) the outflow from a planar slot, or (b) the curtain flow, which both take place in the film coating process. In both cases, a set of $N$ different fluids are superposed and flow together without mixing. We assume that the fluids are Newtonian and incompressible, and that the flows are steady, two-dimensional, and isothermal. Symbols $\rho^{(i)}$ and $\mu^{(i)}$ denote the specific mass and viscosity of fluid number $i$ ($1 \leqslant i \leqslant N = 3$, here).

The liquid–atmosphere and liquid–liquid interfaces are unknown free boundaries. Fluid numbering is performed in such a way that layers $(i)$ and $(i+1)$ are separated by interface $(i)$, where a constant surface tension $\sigma^{(i)}$ is acting. Indexes $i = N$ and possibly $i = 0$ stand for the liquid–atmosphere interfaces.

*Basic Equations*

We must solve the Navier–Stokes and continuity equations in each flow subdomain $\Omega^{(i)}$:

$$\begin{aligned} \rho^{(i)}\mathbf{v}\cdot\nabla\mathbf{v} + \nabla p - \mu^{(i)}\Delta\mathbf{v} &= \mathbf{0}, \\ \nabla\cdot\mathbf{v} &= 0, \qquad \mathbf{x}\in\Omega^{(i)}, \end{aligned} \tag{1}$$

where symbols $\mathbf{v}$, $\nabla$, and $\Delta$ stand for the velocity field, and the gradient and Laplacian operators, respectively, while $p$ denotes the reduced pressure, i.e., the difference between real ($P$) and hydrostatic ($-V^{(i)}$) pressures:

$$p = P + V^{(i)}, \tag{2}$$

with

$$V^{(i)} = -\rho^{(i)}\mathbf{g}\cdot\mathbf{x}, \tag{3}$$

where $\mathbf{g}$ is the acceleration of gravity (981 cm/s$^2$). The method allows us to disregard body forces in (1.1).

Suitable boundary conditions must be imposed. The velocity field vanishes along the fixed walls $\partial\Omega_w$:

$$\mathbf{v} = \mathbf{0}, \qquad \mathbf{x}\in\partial\Omega_w. \tag{4}$$

In the sequel, symbols $\mathbf{n}$ and $\mathbf{s}$ will denote the outgoing normal and tangent unit vectors (for a counterclockwise oriented boundary), while $\mathbf{t}$ represents the reduced contact force on $\partial\Omega$:

$$\mathbf{t} = -p\mathbf{n} + 2\mu^{(i)}\,\mathbf{D}\cdot\mathbf{n}, \tag{5}$$

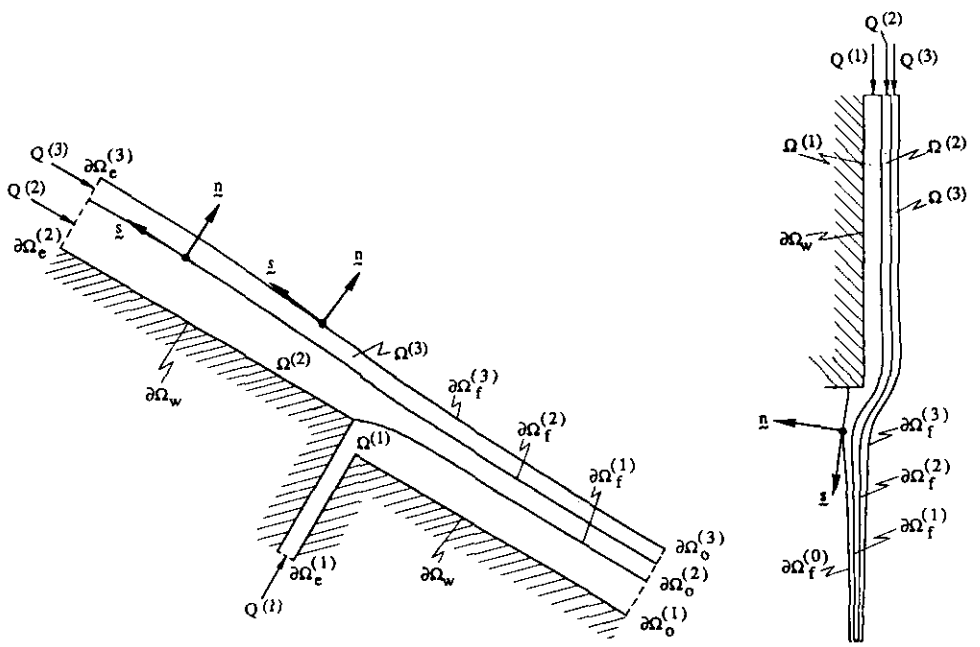


FIG. 1. Schematic description of the problem.

with

$$\mathbf{D} = \tfrac{1}{2}(\nabla \mathbf{v} + \nabla \mathbf{v}^{\mathrm{T}}). \tag{6}$$

We assume zero atmospheric pressure (in the case of slide coating, extension of our method to the situation of a different pressure acting on the upper and lower free surface is straightforward). Hence, kinematic and force equilibrium conditions on the free liquid–atmosphere interfaces $\partial\Omega_f^{(i)}$ ($i=0$ or $N$) are written as

$$\begin{aligned} &\mathbf{v}\cdot\mathbf{n} = 0, \\ &\mathbf{t}\cdot\mathbf{n} + V^{(i)} + \sigma^{(i)}\chi(s) = 0, \\ &\mathbf{t}\cdot\mathbf{s} = 0, \qquad \mathbf{x}\in\partial\Omega_f^{(i)}, \end{aligned} \tag{7}$$

where $\chi(s)$ is the mean curvature at curvilinear abscissa $s$, its sign being positive at the points of $\partial\Omega$ where $\Omega$ is locally convex. In a similar fashion, let $\mathbf{n}$, $\mathbf{s}$, and $\chi(s)$ be defined with respect to layer $(i)$ along the interface $\partial\Omega_f^{(i)}$ separating liquids $(i)$ and $(i+1)$ ($i\neq 0$ or $N$). Let the reduced contact forces $\mathbf{t}^{(i)}$ and $\mathbf{t}^{(i+1)}$ be given by the formulae

$$\begin{aligned} \mathbf{t}^{(i)} &= -p\mathbf{n} + 2\mu^{(i)}\,\mathbf{D}\cdot\mathbf{n}, \\ \mathbf{t}^{(i+1)} &= -p\mathbf{n} + 2\mu^{(i+1)}\,\mathbf{D}\cdot\mathbf{n}, \end{aligned} \tag{8}$$

where $p$ and $\mathbf{D}$ are calculated in layer $(i)$ for $\mathbf{t}^{(i)}$, and in layer $(i+1)$ for $\mathbf{t}^{(i+1)}$. This means that $(\mathbf{t}^{(i)} + V^{(i)}\mathbf{n})$ is the contact force exerted by interface $\partial\Omega_f^{(i)}$ on layer $(i)$, while $(\mathbf{t}^{(i+1)} + V^{(i+1)}\mathbf{n})$ is the contact force exerted on this interface by layer $(i+1)$. Conditions on $\partial\Omega_f^{(i)}$ are written as

$$\begin{aligned} &\mathbf{v}^{(i)}\cdot\mathbf{n} = 0, \\ &\mathbf{v}^{(i+1)}\cdot\mathbf{n} = 0, \\ &(\mathbf{v}^{(i)} - \mathbf{v}^{(i+1)})\cdot\mathbf{s} = 0, \\ &(\mathbf{t}^{(i)} - \mathbf{t}^{(i+1)})\cdot\mathbf{n} + (V^{(i)} - V^{(i+1)}) + \sigma^{(i)}\chi(s) = 0, \\ &(\mathbf{t}^{(i)} - \mathbf{t}^{(i+1)})\cdot\mathbf{s} = 0, \qquad \mathbf{x}\in\partial\Omega_f^{(i)}. \end{aligned} \tag{9}$$

*Inlet and Outlet Conditions*

The flow rate $Q^{(i)}$ within each layer is given. Entry and outlet sections ($\partial\Omega_e^{(i)}$ and $\partial\Omega_o^{(i)}$) are located far enough from the main flow region, in order that velocity profiles be fully developed or that asymptotic curtain flow behavior be achieved. Hence, on any channel entry section, we may write

$$\begin{aligned} &\mathbf{v}\cdot\mathbf{n} = \bar{v}_n(s), \\ &\mathbf{v}\cdot\mathbf{s} = 0, \qquad \mathbf{x}\in\partial\Omega_e^{(i)}, \end{aligned} \tag{10}$$

where $\bar{v}_n(s)$ is a known function of $s$. As inlet conditions on any variable entry section, we impose parallel flow and uniform normal reduced contact force:

$$\begin{aligned} &\mathbf{v}\cdot\mathbf{s} = 0, \\ &\mathbf{t}\cdot\mathbf{n} = c^{(i)}, \qquad \mathbf{x}\in\partial\Omega_e^{(i)}. \end{aligned} \tag{11}$$

The additional unknowns $c^{(i)}$ will be determined from the knowledge of the flow rate:

$$\int_{\partial\Omega_e^{(i)}} \mathbf{v}\cdot\mathbf{n}\,ds + Q^{(i)} = 0. \tag{12}$$

This way of writing the entry conditions is flexible, since it permits us not to impose at the outset the layer thicknesses and the inlet velocity profiles, which result from the calculations. On the inlet sections, data are thus reduced to the flow rates $Q^{(i)}$. Parametric studies are easy, since any solution having converged with a given set of parameters may initialize the iterative process of a different problem, without requiring any preliminary correction of the layer thicknesses.

Two kinds of boundary conditions are used on variable outlet sections. In case (a), we prescribe a zero tangential velocity and the normal stress profile. However, in order to keep the full advantage of obtaining the layer thicknesses as part of the result, the latter condition is imposed through an equivalent procedure: at the outlet, the normal component of the reduced contact force $\mathbf{t}$ (as defined by (5) and (6)) is forced to be constant for any layer; moreover, continuity of the real normal stress profile is assumed and zero normal stress is imposed at the liquid–atmosphere interface. Hence, introducing unknown constants $k^{(i)}$, we write

$$\begin{aligned} &\mathbf{v}\cdot\mathbf{s} = 0, \\ &\mathbf{t}\cdot\mathbf{n} = k^{(i)}, \qquad \mathbf{x}\in\partial\Omega_o^{(i)}, \end{aligned} \tag{13}$$

and

$$\begin{aligned} k^{(i)} + V^{(i)} &= \begin{cases} k^{(i+1)} + V^{(i+1)} & (i\neq N), \\ 0 & (i=N), \end{cases} \\ &\mathbf{x} = \partial\Omega_o^{(i)} \cap \partial\Omega_f^{(i)}. \end{aligned} \tag{14}$$

Conditions (13.2) and (14) are equivalent to prescribing a hydrostatic normal stress profile on $\partial\Omega_o^{(i)}$.

On the other hand, in case (b), we impose a vanishing reduced contact force at the bottom of the curtain:

$$\mathbf{t} = \mathbf{0}, \qquad \mathbf{x}\in\partial\Omega_o^{(i)}. \tag{15}$$

This condition is derived from the curtain flow asymptotic solution (Clarke [13]). Indeed, the latter shows that liquid particles tend to fall as free solid bodies under gravity, provided the curtain height is sufficient.

*Interface Extremity Conditions*

Whenever surface tension is present, additional conditions must be prescribed at the interface extremities in order to define a well-posed problem. Let $R_i$ and $S_i$ be the upstream and downstream extremities of interface $(i)$, respectively, and $\theta_{R_i}$ and $\theta_{S_i}$ denote the angles formed by this interface with the boundary $\partial\Omega$ of the domain. Angles are defined within layer $(i)$, if $i \neq 0$, and within layer (1), if $i = 0$, and are counted as positive or negative depending on whether the tangent $\mathbf{s}$ to the interface $\partial\Omega_f^{(i)}$ is entering or leaving the flow domain (Fig. 2). At any wall–interface intersection, a static contact angle $\bar{\theta}_{R_i}$ is given by the physics of the problem. Hence, the additional condition is written as

$$\theta_{R_i} = \bar{\theta}_{R_i} \qquad \text{at } R_i, \qquad \text{if} \quad \sigma^{(i)} \neq 0. \tag{16}$$

However, in the vicinity of a sharp corner (Fig. 3), the correct result must be selected from among three different solutions, since the interface may separate from the wall (i) at, (ii) below, (iii) above the sharp corner. Note that in case (i), condition (16) is replaced by

$$R_i = \bar{R}_i, \qquad \text{if} \quad \sigma^{(i)} \neq 0, \tag{17}$$

where $\bar{R}_i$ is the sharp edge location. The selection is performed as follows: solution (i) generally exists, but will be retained only when satisfying the Gibbs inequalities:

$$|\bar{\theta}_{R_i}| \leqslant |\theta_{R_i}| \leqslant |\bar{\theta}_{R_i}| + (\pi - \alpha_i), \tag{18}$$

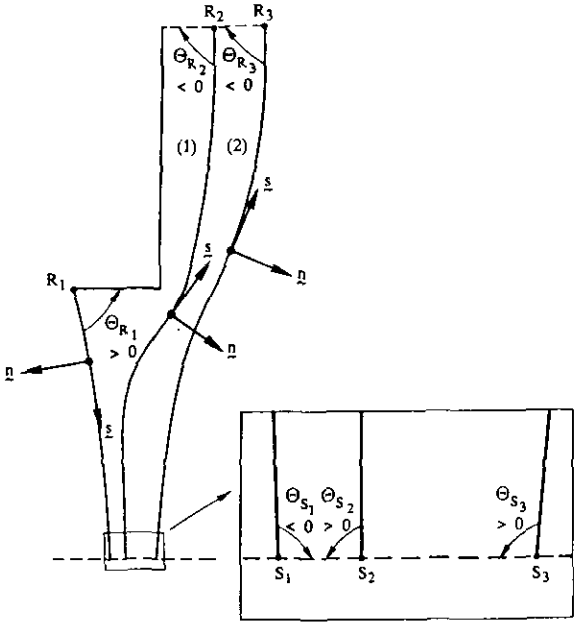


FIG. 2. Definition of the angles $\theta_{R_i}$ and $\theta_{S_i}$.

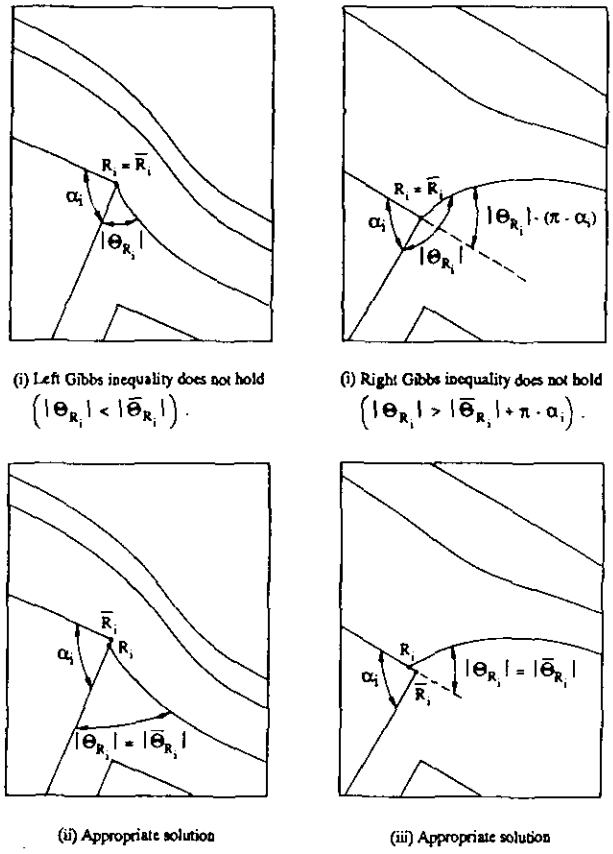


FIG. 3. Obtention of the solution for a non-vanishing interface tension, according to the requirements of the Gibbs inequalities.

where $\alpha_i$ is the sharp edge aperture (these conditions mean that a sharp edge is the limiting case of a rounded edge of smaller and smaller radius of curvature). When either the left or the right inequality of (18) does not hold, a solution of respectively class (ii) or (iii) must be sought.

At any interface extremity belonging to an inflow or outflow section, a non-vanishing surface tension $\sigma^{(i)}$ requires imposing an additional condition of the form (16) (with $\bar{\theta}_{R_i} = \pi/2$), or of the form

$$\theta_{S_i} = \bar{\theta}_{S_i} \qquad (= \pm\pi/2), \qquad \text{if} \quad \sigma^{(i)} \neq 0. \tag{19}$$

Inflow and outflow sections are indeed asymptotically perpendicular to the tilted plane or to the curtain. These conditions are necessary in order to discard unwanted solutions which have zero or singular velocity at the interface extremity (Fig. 4). As concentrated capillary forces are present within the interface, but not within the inlet or outlet section, such solutions could be obtained by exerting a non-vanishing force on the extremity. In this case, non-right angles $\theta_{R_i}$ or $\theta_{S_i}$ result from force equilibrium along the section at $R_i$ or $S_i$ (Moffat [14]).

The problem is more difficult when a given interface tension vanishes. For real non-miscible fluids, zero tension

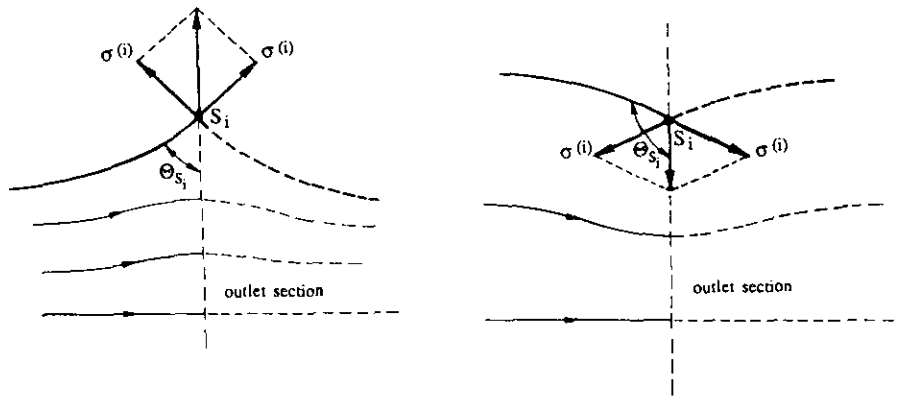


FIG. 4. Influence of exerting a normal force on the interface extremity.

is an approximation of a non-zero, but very low, value of this parameter. Hence, the approximating model should be obtained by letting interface tension tend to zero in a family of approaching situations. A singular perturbation problem is obtained in this way, since additional conditions are no longer required at interface extremities when surface tension vanishes. In particular, the location of a wall–interface intersection or the value of a separation angle are functions of the flow parameters and cannot be imposed.

Nonetheless, at zero surface tension, additional extremity conditions are often used in literature for facilitating the obtention of numerical solutions, whenever they seem to be likely or justified by analytical analysis. Let us point out that, for a closed mathematical system (which here is the case), additional conditions are allowed only provided they are involved by the model. Pressure continuity at an interface extremity is, for example, used by Scanlan and Scriven [15]. However, the validity of this statement is not clear, since regularity of the interface and the pressure field is assumed in the proof which is, therefore, not complete: infinite curvature of the interface at the extremity cannot be a priori discarded at zero tension. In this case, when letting surface tension tend to zero to obtain the solution, the product of interface tension and interface curvature might not tend to zero at the extremity, and a similar behavior might be observed for the pressure jump across the interface, since the latter is related to this product by Eqs. (8) and (9.4). Let us also mention that pressure singularity is possible even with a regular interface if the latter is tangent to the wall at the extremity ($|\bar{\theta}_{R_i}| = 0$ or $\pi$) (Michael [16]). For these reasons, no additional extremity condition such as pressure continuity was used in the present work. The validity of our approach has been confirmed by further numerical experiments (Levieux *et al.* [17]), which have exhibited a very likely singular behavior of the solution in the vicinity of the interface extremity. Only a change in the model could remove this mathematical singularity.

A second example of a useful simplifying condition at zero tension consists in forcing, when likely, a wall–interface intersection to be located at a sharp edge. This method, which is used in Section 4, is justified by the strong attraction exerted by the sharp edge on the interface extremity, as will be shown further by some examples. The present state of the theory does not say whether the exact intersection is located at the sharp edge either within a range of values of the flow parameters (as in the case of a non-vanishing interface tension) or for isolated values of these parameters. However, according to the numerical experiments of Levieux *et al.* [17], the latter behavior seems to be observed. Nevertheless, even if the exact interface is not originating from the sharp edge, locating the approximate interface origin on this edge may be useful, since we must distinguish between numerical and analytical solutions: if the distance between a sharp edge and the exact origin is much smaller than the local mesh size, better approximate solutions will be provided by this method.

### 2.2. Weak Formulation

The problem to solve may be written as

$$G(X) = 0, \tag{20}$$

where $X$ represents the set of unknowns, including the free boundaries. A weak formulation is required for using the Galerkin finite element method, in order to allow the approximate solution to be less regular than if a strong formulation were used. In general, weak formulations are written as

(WF) Find $X \in \Psi$ such that, for any test-function $\delta Y$ belonging to the tangent space $\Xi(X)$ to $\Psi$ at $X$, a suitable inner product $\delta M$ of $G(X)$ and $\delta Y$ vanishes,

$$\delta M = \langle G(X), \delta Y \rangle = 0. \tag{21}$$

It will indeed be shown that, for free surface problems, the linear space $\Xi(X)$ is not constant.

In the present case, unknowns are both a set of curves (i.e., the interfaces $\partial\Omega_f^{(i)}$, $i=0$ to $N$) and a set of functions which are defined on variable domains depending on these curves. In particular, unknowns include the velocity and reduced pressure fields. We require that the reduced pressure belongs to the $L^2(\Omega)$ set of functions which have a summable square over the flow domain $\Omega = \bigcup_i \Omega^{(i)}$. Within each subdomain $\Omega^{(i)}$, we also impose that velocities belong to the $H_1(\Omega^{(i)})$ Sobolev space of functions whose gradient has a summable square over $\Omega^{(i)}$. Moreover, velocities are constrained to satisfy essential conditions (4) and (10). In general, we prescribe that all functions and free curves are regular enough to give a sense to the integrals involved (see also Dupret [7]).

A peculiar feature of our method lies in introducing additional unknowns (or Lagrange multipliers) which are defined either along the liquid–atmosphere interfaces,

$$\lambda_n = \mathbf{t}\cdot\mathbf{n}, \qquad \mathbf{x}\in\partial\Omega_f^{(i)} \qquad (i=0 \text{ or } N), \tag{22}$$

or along the liquid–liquid interfaces,

$$\begin{aligned} \lambda_n^- &= \mathbf{t}^{(i)}\cdot\mathbf{n}, \\ \lambda_n^+ &= \mathbf{t}^{(i+1)}\cdot\mathbf{n}, \\ \lambda_s &= \mathbf{t}^{(i)}\cdot\mathbf{s} = \mathbf{t}^{(i+1)}\cdot\mathbf{s}, \\ &\mathbf{x}\in\partial\Omega_f^{(i)} \qquad (i=1 \text{ to } N-1), \end{aligned} \tag{23}$$

or along the inlet and outlet free sections,

$$\lambda_s = \mathbf{t}\cdot\mathbf{s}, \qquad \mathbf{x}\in\partial\Omega_e^{(i)} \text{ or } \partial\Omega_o^{(i)} \qquad (i=1, \ldots, N). \tag{24}$$

We shall see that Lagrange multipliers provide an efficient way of imposing kinematic conditions along the free boundaries. According to this approach, velocity continuity across the interfaces is not imposed in a strong, but in a weak sense. The technique will be justified in Section 3.3.

*Construction of the Weak Formulation*

Let us now step by step build a weak formulation of the problem. The variational form $\delta M$ involved in (21) will be a sum,

$$\delta M = \delta M_1 + \delta M_2 + \delta M_3. \tag{25}$$

The first term $\delta M_1$ is defined as

$$\begin{aligned} \delta M_1 = \sum_i \int_{\Omega^{(i)}} [&\rho^{(i)}\mathbf{v}\cdot\nabla\mathbf{v}\cdot\delta\mathbf{v} \\ &+ 2\mu^{(i)}\,\mathbf{D}:\delta\mathbf{D} - \delta(p\nabla\cdot\mathbf{v})]\,d\sigma, \end{aligned} \tag{26}$$

where $\delta p(\mathbf{x})$ and $\delta\mathbf{v}(\mathbf{x})$ are arbitrary test functions (which are part of $\delta Y$), while $\delta\mathbf{D}$ is given by

$$\delta\mathbf{D} = \tfrac{1}{2}(\nabla\,\delta\mathbf{v} + \nabla\,\delta\mathbf{v}^{\mathrm{T}}), \tag{27}$$

and $\delta(p\nabla\cdot\mathbf{v})$ is defined from the shortened notation

$$\delta(ab) = a(\delta b) + (\delta a)\,b. \tag{28}$$

Test functions $\delta p(\mathbf{x})$ belong to the $L^2(\Omega)$ space, while test functions $\delta\mathbf{v}(\mathbf{x})$ belong to the $H_1(\Omega^{(i)})$ space within each subdomain $\Omega^{(i)}$ and are constrained to vanish along each part of the boundary where velocities are imposed by (4) and (10):

$$\delta\mathbf{v}(\mathbf{x}) = \mathbf{0}, \qquad \mathbf{x}\in\partial\Omega_w \text{ or } \partial\Omega_e^{(i)} \text{ (if fixed)}. \tag{29}$$

Integration by parts shows that the weak formulation (21) implies that the strong equations (1) be satisfied for regular unknown functions. From (5), (6), and (27), and taking (29) into account, (26) yields

$$\delta M_1 = \delta M_1^d + \delta M_1^f + \delta M_1^e + \delta M_1^o, \tag{30}$$

with

$$\begin{aligned} \delta M_1^d = \sum_i \int_{\Omega^{(i)}} [&(\rho^{(i)}\mathbf{v}\cdot\nabla\mathbf{v} \\ &+ \nabla p - \mu^{(i)}\,\Delta\mathbf{v})\cdot\delta\mathbf{v} - \nabla\cdot\mathbf{v}\,\delta p]\,d\sigma, \end{aligned} \tag{31}$$

$$\begin{aligned} \delta M_1^f = &\sum_{\substack{i=0 \text{ or } N \\ (\partial\Omega_f^{(i)} \text{ free})}} \int_{\partial\Omega_f^{(i)}} \mathbf{t}\cdot\delta\mathbf{v}\,ds \\ &+ \sum_{i\neq 0,\,N} \int_{\partial\Omega_f^{(i)}} (\mathbf{t}^{(i)}\cdot\delta\mathbf{v}^{(i)} \\ &- \mathbf{t}^{(i+1)}\cdot\delta\mathbf{v}^{(i+1)})\,ds, \end{aligned} \tag{32}$$

$$\delta M_1^e = \sum_{\substack{i=1 \\ (\partial\Omega_e^{(i)} \text{ free})}}^{N} \int_{\partial\Omega_e^{(i)}} \mathbf{t}\cdot\delta\mathbf{v}\,ds, \tag{33}$$

$$\delta M_1^o = \sum_{i=1}^{N} \int_{\partial\Omega_o^{(i)}} \mathbf{t}\cdot\delta\mathbf{v}\,ds. \tag{34}$$

Letting $\delta M$ vanish for any test function $\delta Y$ causes $\delta M_1^d$ to vanish for any $\delta p$ and any particular $\delta\mathbf{v}$ which vanishes along each $\partial\Omega^{(i)}$, since $\delta M$ reduces to $\delta M_1^d$ in this case. Hence, (1) is satisfied within each subdomain $\Omega^{(i)}$.

The second term $\delta M_2$ of $\delta M$ in (25) is a sum,

$$\begin{aligned} \delta M_2 &= \delta M_2^f + \delta M_2^e + \delta M_2^o \qquad \text{(case (a))}, \\ \delta M_2 &= \delta M_2^f + \delta M_2^e \qquad\qquad\quad \text{(case (b))}, \end{aligned} \tag{35}$$

with

$$\delta M_2^f = -\sum_{\substack{i=0 \text{ or } N \\ (\partial\Omega_f^{(i)} \text{ free})}} \int_{\partial\Omega_f^{(i)}} \delta(\lambda_n v_n)\, ds - \sum_{i \neq 0, N} \int_{\partial\Omega_f^{(i)}} \delta(\lambda_n^- v_n^{(i)} - \lambda_n^+ v_n^{(i+1)} + \lambda_s(v_s^{(i)} - v_s^{(i+1)}))\, ds, \tag{36}$$

$$\delta M_2^c = -\sum_{\substack{i=1 \\ (\partial\Omega_c^{(i)} \text{ free})}}^{N} \left\{ \int_{\partial\Omega_c^{(i)}} \delta(c^{(i)} v_n + \lambda_s v_s)\, ds - Q^{(i)}\, \delta c^{(i)} \right\}, \tag{37}$$

$$\delta M_2^\sigma = -\sum_{i=1}^{N} \int_{\partial\Omega_a^{(i)}} [k^{(i)}\, \delta v_n + \delta(\lambda_s v_s)]\, ds + \sum_{i=1}^{N-1} (k^{(i)} - k^{(i+1)} + V^{(i)} - V^{(i+1)})_{S^i}\, \delta k^{(i)} + (k^{(N)} + V^{(N)})_{S^N}\, \delta k^{(N)}, \tag{38}$$

where $\delta\lambda_n(s)$, $\delta\lambda_n^+(s)$, $\delta\lambda_n^-(s)$, $\delta\lambda_s(s)$ are arbitrary test functions (belonging to suitable functional spaces), while $\delta c^{(i)}$ and $\delta k^{(i)}$ are arbitrary numbers, all being part of $\delta Y$. Shortened notations (28) and

$$\delta(a+b) = \delta a + \delta b \tag{39}$$

are used.

The weak formulation (21) involves boundary and interface conditions (7.1), (7.3), (9.1), (9.2), (9.3), (9.5), (11) to (14), and (22) to (24) to be satisfied for regular unknown functions. This may easily be shown by adding Eqs. (32) and (36), (33) and (37), and (34) and (38), respectively, and by recalling that (31) has been proved to vanish. The expected result follows by letting the terms in $\delta v_n$, $\delta v_s$, $\delta\lambda_n$, ... vanish successively in $(\delta M_1 + \delta M_2)$. We should emphasize here that our weak formulation of free inlet and outlet conditions is very efficient, since only the flow rates $Q^{(i)}$ need to be imposed.

The last term $\delta M_3$ of $\delta M$ is the sum

$$\delta M_3 = \delta M_3^\lambda + \delta M_3^\sigma + \delta M_3^\gamma, \tag{40}$$

with

$$\delta M_3^\lambda = -\sum_{\substack{i=0 \text{ or } N \\ (\partial\Omega_f^{(i)} \text{ free})}} \int_{\partial\Omega_f^{(i)}} (\lambda_n + V^{(i)})\, \delta\alpha\, ds - \sum_{i \neq 0, N} \int_{\partial\Omega_f^{(i)}} (\lambda_n^- - \lambda_n^+ + V^{(i)} - V^{(i+1)})\, \delta\alpha\, ds, \tag{41}$$

$$\delta M_3^\sigma = \sum_{\substack{i \\ (\partial\Omega_f^{(i)} \text{ free})}} \left\{ \int_{\partial\Omega_f^{(i)}} \sigma^{(i)} \phi \frac{d\,\delta\alpha}{ds}\, ds - [\sigma^{(i)} \phi\, \delta\alpha]_{\partial\Omega_f^{(i)}} \right\}, \tag{42}$$

$$\delta M_3^\gamma = \sum_{\substack{i \\ (\partial\Omega_f^{(i)} \text{ free})}} [\sigma^{(i)}(\cos\theta - \cos\bar{\theta})\, \delta\gamma]_{\partial\Omega_f^{(i)}}, \tag{43}$$

where $\delta\alpha(s)$ is an arbitrary test function (part of $\delta Y$) which is constrained to vanish at any fixed interface extremity, and $\phi(s)$ denotes the angle between the normal $\mathbf{n}$ and the horizontal direction (Fig. 5). The symbol $\delta\gamma$ is defined by

$$\delta\gamma = \delta\alpha/\sin\theta, \qquad \text{at } R_i \text{ or } S_i, \tag{44}$$

and is used to simplify the notations (see Dupret [8]).

From the identity

$$\chi(s) = \frac{d\phi}{ds}, \qquad \mathbf{x} \in \partial\Omega_f^{(i)}, \tag{45}$$

it is easy to integrate (42) by parts:

$$\delta M_3^\sigma = -\sum_{\substack{i \\ (\partial\Omega_f^{(i)} \text{ free})}} \int_{\partial\Omega_f^{(i)}} \sigma^{(i)} \chi\, \delta\alpha\, ds. \tag{46}$$

Hence, letting $\delta M$ vanish, from (21), for any $\delta Y$ causes $(\delta M_3^\lambda + \delta M_3^\sigma)$ to vanish for any particular $\delta\alpha$ which is zero at the interface extremities, since $\delta M$ then reduces to $(\delta M_3^\lambda + \delta M_3^\sigma)$. From (46), this shows that boundary and interface conditions (7.2) and (9.4) are satisfied for regular unknowns. As $\delta M$ then reduces to $\delta M_3^\gamma$, letting, in (43), the terms in $\delta\gamma(R_i)$ and $\delta\gamma(S_i)$ vanish shows that extremity conditions (16) and (19) are satisfied (if $R_i$ is not fixed).

Introduction of capillary conditions via Eqs. (45) and (42) was performed in Dupret [8] on the basis of a variational approach. This method differs from the one of Ruschak [11], with the advantages of allowing a greater freedom in the selection of interpolating functions (through the use of Lagrange multipliers) and of allowing an easy treatment of static contact angles.

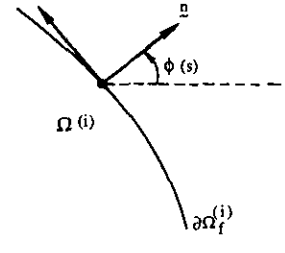


FIG. 5. Definition of the angle $\phi(s)$.

## 3. NUMERICAL METHOD

### 3.1. Discretization

From the weak formulation (21), equations are easily made discrete by defining suitable subspaces $\Psi^*$ and $\Xi^*(X)$ of $\Psi$ and $\Xi(X)$. Following the Galerkin finite element method (Strang and Fix [18], Zienkiewicz [19]), these are obtained by introducing appropriate global shape functions $\omega_k(\mathbf{x})$, $\pi_m(\mathbf{x})$, $v_q(s)$, and $\chi_r(s)$, and by using the following approximations:

$$\begin{aligned}
\mathbf{v}(\mathbf{x}) &= \sum_k \mathbf{v}_k \omega_k(\mathbf{x}), \\
\delta\mathbf{v}(\mathbf{x}) &= \sum_k \delta\mathbf{v}_k \omega_k(\mathbf{x}), \\
p(\mathbf{x}) &= \sum_m p_m \pi_m(\mathbf{x}), \\
\delta p(\mathbf{x}) &= \sum_m \delta p_m \pi_m(\mathbf{x}), \qquad \mathbf{x} \in \Omega^{(i)},
\end{aligned} \tag{47}$$

$$\begin{aligned}
\lambda(s) &= \sum_q \lambda_q v_q(s), \\
\delta\lambda(s) &= \sum_q \delta\lambda_q v_q(s), \qquad \mathbf{x} \in \text{free } \partial\Omega_f^{(i)} \\
&\qquad\qquad \text{or free } \partial\Omega_e^{(i)} \text{ or } \partial\Omega_o^{(i)},
\end{aligned} \tag{48}$$

$$\begin{aligned}
\mathbf{x}(s) &= \sum_r \mathbf{x}_r \chi_r(s), \\
\delta\alpha(s) &= \sum_r \delta\alpha_r \chi_r(s), \qquad \mathbf{x} \in \text{free } \partial\Omega_f^{(i)}.
\end{aligned} \tag{49}$$

In the latter, symbols $\mathbf{v}_k$, $p_m$, $\lambda_q$, and $\mathbf{x}_r$ stand for the unknown nodal values, while $\delta\mathbf{v}_k$, $\delta p_m$, $\delta\lambda_q$, and $\delta\alpha_r$ are arbitrary numbers (or vectors), each of them being associated with a particular equation (or couple of equations) of the system. For the sake of brevity, a common symbol $\lambda(s)$ is used for representing all the different Lagrange multipliers $\lambda_n(s)$, $\lambda_n^+(s)$, ... defined on the interfaces and the free inlet and outlet sections.

In order to approximate the velocity and pressure fields, we use quadratic or biquadratic, and linear or bilinear polynomials, respectively, on the triangular or quadrilateral parent element. As discussed in the previous section, velocities and pressure are not imposed to be continuous on the fluid–fluid interfaces, where nodes are thus doubled (recall from Section 2.2 that velocity continuity is imposed in a weak sense).

*Peculiar Discretization on the Interfaces*

Extensive freedom is allowed in selecting appropriate shape functions for the Lagrange multipliers and the coordinates. The variational method which is used for solving the system, however, imposes that all these functions be continuous. Following Babuška [10], mesh convergence is improved by using linear Lagrange multipliers. Moreover, curved interface boundaries are preferred to piecewise rectilinear ones when surface tension is present. Therefore, our basic option consists of using, on the one-dimensional parent element, piecewise linear shape functions for the Lagrange multipliers, and piecewise quadratic shape functions for the coordinates and the test functions $\delta\alpha(s)$. Element sides may thus be curved along the interfaces.

However, as liquid–liquid interface tension is normally neglected, Eqs. (21), (25), (40) to (43), and (44) imply that equality

$$-\int_{\partial\Omega_f^{(i)}} (\lambda_n^- - \lambda_n^+ + V^{(i)} - V^{(i+1)})\, \delta\alpha\, ds = 0 \qquad (i \neq 0, N), \tag{50}$$

must hold for any test function $\delta\alpha(s)$. In this case, selecting our basic option for discretizing $\lambda_n^-(s)$, $\lambda_n^+(s)$, and $\delta\alpha(s)$ will lock the system, since an interface formed by $m$ one-dimensional elements has $(m+1)$ nodes both for $\lambda_n^-$ and $\lambda_n^+$, and $(2m+1)$ nodes for $\delta\alpha$. Hence, Eq. (50) yields $(2m+1)$ equations, where the unknowns may be grouped in the $(m+1)$ nodal differences $(\lambda_n^- - \lambda_n^+)$. Such a system is clearly impossible, but it can be unlocked by using quadratic shape functions for the Lagrange multipliers $\lambda_n^-$ and $\lambda_n^+$. Unfortunately, a new locking mode may be found, since Eqs. (21), (25), (35), and (36) imply that equality

$$-\int_{\partial\Omega_f^{(i)}} (\delta\lambda_n^- v_n^{(i)} - \delta\lambda_n^+ v_n^{(i+1)} + \delta\lambda_s (v_s^{(i)} - v_s^{(i+1)}))\, ds = 0 \qquad (i \neq 0, N) \tag{51}$$

must hold for arbitrary test functions $\delta\lambda_n^-(s)$, $\delta\lambda_n^+(s)$, and $\delta\lambda_s(s)$. If the upstream interface extremity is free on the fixed wall $\partial\Omega_w$, there are eight nodal velocities on the interface extremity and the adjacent midside node (as velocities are discontinuous on the interface), while there are four essential conditions (4), plus five equations resulting from (51), which must be satisfied by these eight unknowns. Finally, the system is unlocked by using, on the liquid–liquid interface sides which are adjacent to the boundary $\partial\Omega$, linear shape functions for $\lambda_n^-(s)$, $\lambda_n^+(s)$, and $\delta\alpha(s)$. The same discretization could be used over the entire interfaces, but the results are of lower quality. Let us mention that a particular treatment of the interface was also used by Dheur and Crochet [20] in the vicinity of the separation line when surface tension vanishes.

On any interface, from (49), the number of interface coordinate nodes $\mathbf{x}_r$ is exactly the number of arbitrary $\delta\alpha_r$, i.e., the number of degrees of freedom of the test function $\delta\alpha(s)$. In order to obtain the same number of equations and unknowns, interface coordinate nodes are constrained to

fixed straight lines or circles, whose equations may be written in the form

$$A_r x + B_r y - C_r(x^2 + y^2) = D_r. \tag{52}$$

These loci differ from free spines (Ruschak [11], Kistler [5]), since only interface nodes are constrained, and they must be constructed in such a manner that the expected interface deformation be possible. Data introduction is facilitated by introducing in a first stage only a few constraining lines, while any locus which remains undefined is calculated by linear interpolation on the coefficients $A_r$, $B_r$, $C_r$, and $D_r$ of the couple of enclosing and already defined loci. Bundles of parallel or convergent straight lines, or of circles of the same radical axis, are thus obtained. Examples are shown in Fig. 6, where the particular case of a fixed interface extremity, whose locus is a circle of vanishing radius, must be emphasized.

The system of discretized equations must be completed by describing how the meshes are deformed. The technique, which consists in moving internal nodes according to the displacement of the interfaces, is described in the next subsection. Note that only rectilinear internal sides are accepted.

### 3.2. Mesh Conditioning

In order to provide accurate solutions, moving meshes must be as well-conformed as possible. However, this objective is severe, since interface shapes are strongly dependent on the parameters of the problem, while the same mesh topology will be used within a wide range of these parameters in order to allow easy parametric studies.

The method which is developed here consists in fixing after displacement, at each iteration, the boundary and interface nodes, and then moving the internal nodes until the mesh is acceptable. This result is obtained by exerting on any internal node a pseudo-force which tends to correct ill-behaved elements and which vanishes for a satisfactory solution. Hence, the sole problems are to define appropriate pseudo-forces and to build a suitable iterative scheme for obtaining the deformed mesh.

*Definition of Pseudo-Forces*

Consider first the case of straight-sided triangles. Any nodal pseudo-force $\mathbf{F}^{*l}$ is a sum of contributions $\mathbf{F}_k^{*l}$ furnished by the elements which are adjacent to the global vertex $\mathbf{x}^{*l}$:

$$\mathbf{F}^{*l} = \sum_{\substack{k \text{ such that} \\ \text{vertex } l \in \text{element } k}} \mathbf{F}_k^{*l}. \tag{53}$$

For defining all the pseudo-forces, it is sufficient to consider a single triangle. Local vertex numbering may thus be used and $\mathbf{F}^i$ will denote the contribution $\mathbf{F}_k^{*l}$, provided $l$ is the global index of the $i$th vertex of element $k$. It is convenient to use the following notations: symbols $S$, $\phi_i$, and $c_i$ denote the area of the triangle, its $i$th angle, and the length of the opposite side, respectively, while $c_{i1}$ and $c_{i2}$ stand for the lengths of the couple of sides which are adjacent to vertex $\mathbf{x}^i$ (Fig. 7).

A first attempt to define appropriate pseudo-forces $\mathbf{F}^i$ was made by letting the latter derive from a pseudo-energy $E_t$:

$$\mathbf{F}^i = -\nabla^{(i)} E_t, \tag{54}$$

where $\nabla^{(i)}$ denotes the gradient with respect to vertex $i$. Hence, this method consists in minimizing the total pseudo-energy for fixed boundary and interface nodes. The pseudo-energy of a given triangle was defined by the formula

$$E_t = S\left(\sum_{i=1}^{3} \frac{1}{\sin^2 \phi_i} - 4\right). \tag{55}$$

It is easy to show that $E_t$ vanishes and is a minimum when the triangle is equilateral, whatever its area $S$, and that $E_t$ is

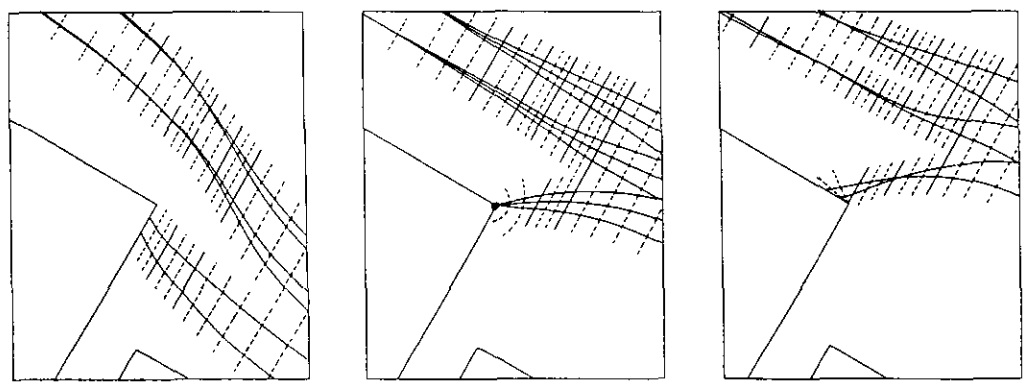

FIG. 6. Constraining lines for the free surface nodes: ———, lines introduced in a first stage; ——, interpolated lines.

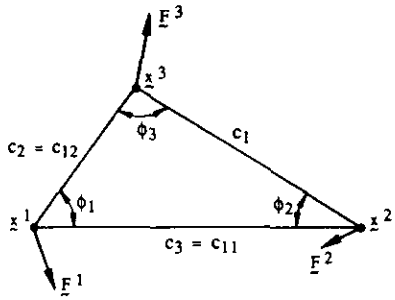


FIG. 7. System of pseudo-forces exerted on a triangle.

infinite for a degenerate triangle with one or two vanishing angles. This means that the best-shaped elements were expected to result. Nonetheless, poor results were observed in some cases, so improvement of the method turned out to be necessary.

Equation (55) may be written as

$$E_t = \frac{1}{2}\sum_{i=1}^{3} c_{i1}c_{i2}\left(\frac{1}{\sin\phi_i} - \frac{4}{3}\sin\phi_i\right). \tag{56}$$

Hence, replacing $c_{i1}$ and $c_{i2}$ by the suitable $c_j$'s and differentiating (56) yields from (54) the formal development

$$\mathbf{F}^i = \mathbf{F}^i_{(s)} + \mathbf{F}^i_{(m)}, \tag{57}$$

with

$$\begin{aligned} \mathbf{F}^i_{(s)} &= -\sum_{j=1}^{3} \frac{\partial E_t}{\partial c_j}\nabla^{(i)}c_j, \\ \mathbf{F}^i_{(m)} &= -\sum_{j=1}^{3} \frac{\partial E_t}{\partial \phi_j}\nabla^{(i)}\phi_j. \end{aligned} \tag{58}$$

Two pseudo-force components are thus set apart. The former $\mathbf{F}^i_{(s)}$ consists of terms which are parallel to the sides $\mathbf{c}_j$ of the triangle, since we may write

$$\nabla^{(i)}c_j = e^i_j \frac{1}{c_j}\mathbf{c}_j, \tag{59}$$

where the coefficient $e^i_j$ is 1, 0, or $-1$, following the values of indexes $i$ and $j$. The latter component $\mathbf{F}^i_{(m)}$ may be interpreted as arising from a set of three pseudo-momenta $M^j$,

$$M^j = \frac{1}{2}c_{j1}c_{j2}\left(\frac{1}{\sin^2\phi_j} + \frac{4}{3}\right)\cos\phi_j, \tag{60}$$

which tend to correct the angles $\phi_j$ of the triangle by opening the acute angles and closing the obtuse ones (Fig. 8).

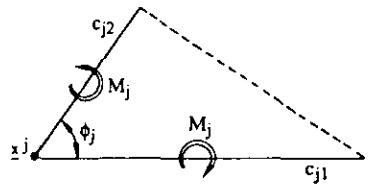


FIG. 8. Pseudo-momenta exerted on a pair of adjacent sides.

Improved solutions were obtained by suppressing the $\mathbf{F}^i_{(s)}$ component of the pseudo-force:

$$\mathbf{F}^i = \mathbf{F}^i_{(m)}. \tag{61}$$

Equilateral triangles remain perfectly shaped (with vanishing pseudo-forces), but the existence of a solution is not strictly ensured, since we no longer have a minimum problem. However, the quality of the results may be explained by observing that pseudo-forces are defined in such a way that small sides do not play a more important role than longer ones. Indeed, according to Eq. (60), the internal pseudo-forces which are associated with two similar triangles are exactly proportional to the sizes of these triangles. Hence, induced displacements will be of the order of magnitude of these respective sizes.

Consider now the case of straight-sided quadrilaterals. On any such element, four triangles are superposed, each of them being formed by the couple of sides (of length $c_{i1}$ and $c_{i2}$) which are adjacent to a given vertex $\mathbf{x}_i$, and by the opposite diagonal (of length $d_i$) (Fig. 9). Formula (56) is extended by defining the pseudo-energy $E_q$ as

$$\begin{aligned} E_q &= \alpha \sum_{i=1}^{4} E^i_q, \\ E^i_q &= \frac{1}{2}c_{i1}c_{i2}\left(\frac{1}{\sin\phi_i} - \beta\sin\phi_i\right) \\ &\quad + \frac{\beta-1}{4(2-\beta)}\sum_{j=1}^{2} c_{ij}d_i\left(\frac{1}{\sin\phi_{ij}} - \beta\sin\phi_{ij}\right), \end{aligned} \tag{62}$$

where $\alpha$ and $\beta$ are suitable parameters ($\alpha > 0$, $1 \leqslant \beta < 2$), and $\phi_{ij}$ ($j = 1, 2$) are the angles at the vertices which are

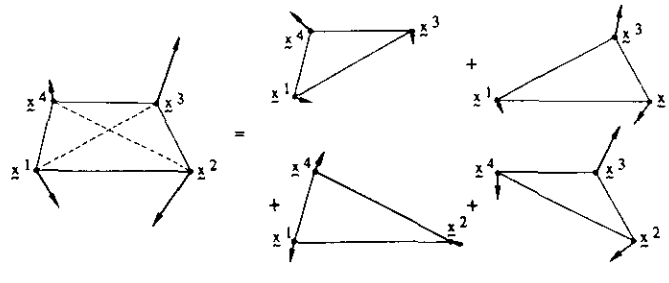


FIG. 9. System of pseudo-forces exerted on a quadrilateral.

adjacent to $\mathbf{x}_i$. Pseudo-forces are obtained in the same way as for triangles, by writing

$$\mathbf{F}^i = \mathbf{F}^i_{(m)} = -\sum_{j=1}^{4}\left[\frac{\partial E_q}{\partial \phi_j}\nabla^{(i)}\phi_j + \sum_{k=1}^{2}\frac{\partial E_q}{\partial \phi_{jk}}\nabla^{(i)}\phi_{jk}\right]. \quad (63)$$

It is possible to show that squares are perfectly shaped, with vanishing pseudo-forces, whatever $\alpha$ and $\beta$. When the value $\beta = 1$ is selected, even rectangles are perfectly shaped. Numerical experiments have shown that good results are otained using the values $\alpha = 3$ and $\beta = 7/6$. This selection provides a suitable pseudo-force ratio between triangles and quadrilaterals, while long and thin rectangles are avoided inside the domain since $\beta$ is not exactly one.

Besides rectilinear sides, curved sides may also be used both in triangles and quadrilaterals, but only along the boundary and the interfaces, whose nodes are fixed during mesh conditioning. Hence, it is clear that pseudo-forces can be calculated exactly as if curved sides were not present.

*Solution Procedure for Mesh Control*

The flow problem is solved using an iterative scheme which will be described in the next subsection. At any iteration, after displacement of the interfaces, mesh conditioning is performed separately by assembling nodal equations,

$$\mathbf{F}^{*l}(\mathbf{x}^{*m}) = \mathbf{0}, \quad (64)$$

and by solving the latter using Newton's method. In order to obtain the first well-conditioned mesh from the initial one before starting the calculations, a particular technique of residual relaxation has been introduced since equations are difficult to solve when mesh deformation is too important. The technique consists in solving instead of (64) a sequence of $N^*$ systems of the form

$$\mathbf{F}^{*l}(\mathbf{x}^{*m}_n) = \omega_n \mathbf{F}^{*l}(\mathbf{x}^{*m}_0) \quad (1 > \omega_1 > \omega_2 > \cdots > \omega_{N^*} = 0), \quad (65)$$

where the symbols $\mathbf{x}^{*m}_0$ represent the initial vertices, while $\mathbf{x}^{*m}_{N^*} = \mathbf{x}^{*m}$ denote the vertices of the corrected mesh. Any intermediate solution $\mathbf{x}^{*m}_{n-1}$ serves as the starting value for solving through Newton's method the new system, whose unknowns are the $\mathbf{x}^{*m}_n$'s.

The method described in this section provides good results. An example of first correction is shown in Fig. 10. Improvements are, of course, possible. However, the general scheme should be retained since the method is fully automatic and can be used without tuning for any mesh topology.

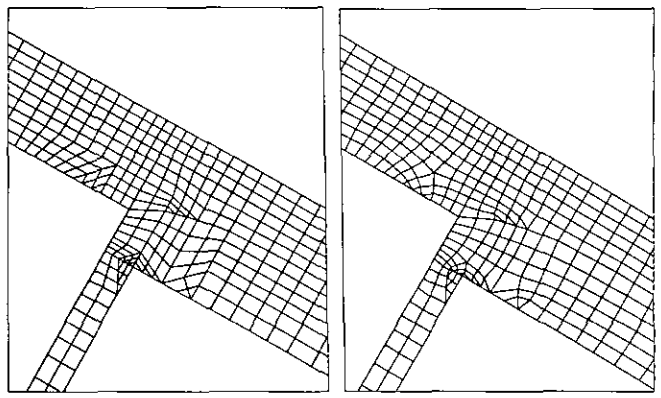

**FIG. 10.** Example of initial and first corrected mesh (note that interfaces are fixed during correction).

### 3.3. Iterative Algorithm

Early methods for solving free-surface problems were based on an iterative scheme using two basic modules. The first one solved, over a fixed domain, a reduced problem obtained by discarding one of the free-surface boundary conditions; the second one determined the new location of the free-surface with the remaining equation. This could be either the kinematic or the normal stress condition. These methods were introduced by Nickell *et al.* [21], and extended by Silliman and Scriven [22] to the case where surface tension is present.

The whole procedure may nonetheless remain too slow, especially when other nonlinearities are present. A faster method is to iterate simultaneously on all the unknowns of the problem. This was first done by Ruschak [11], and is the approach chosen by Saito and Scriven [3], Kistler [5], ... and in the present paper.

Development of a Newton method in the case of a problem in a fixed given domain is quite simple. Suppose the problem has a weak formulation of the form (21). The tangent linear space $\Xi(X)$ is constant. Hence, one has only to fix the test function $\delta Y$ and expand the form $\delta M$ into a series up to the first order. The linear equation to be solved at each iteration and giving the increments $\bar{\delta} X_m$,

$$\bar{\delta} X_m = X_{m+1} - X_m, \quad (66)$$

is of the form

$$\langle H(X_m)\,\bar{\delta} X_m, \delta Y\rangle + \langle G(X_m), \delta Y\rangle = 0, \qquad \forall\, \delta Y \in \Xi, \quad (67)$$

where $H(X)$ is a linear operator. The latter equation may be developed for the continuous problem (21). Discretization, which gives the stiffness matrix, may then be carried out on this continuous form (67).

The case of a free-surface problem is more difficult, because an exact Newton method needs to be developed for the discretized form of the equations (as done by Ruschak [11]). This procedure has provided numerous useful results in the last few years (see, in particular, Saito and Scriven [3], Kistler and Scriven [4], and Kistler [5]). Our solution is different and consists, following Dupret [9], in using a Newton-like method developed for the continuous form (21) of the equations and discretized in a following step.

Exact Newton and our Newton-like methods are basically similar. In both cases, the iterative scheme is derived by linearising the coupled equations of the problem. Convergence rate is quadratic in the former case, and quasi-quadratic in the latter case, which means that convergence is all the more quadratic as long as the approximation is improved (as a consequence of mesh refinement). Indeed, linearisation and discretisation of the weak continuous form of the equations do not exactly commute for a free-surface problem.

Any iteration of our Newton-like scheme consists of four sub-steps:

(i) solution of the coupled linear system, which provides velocity and pressure nodal increments at fixed locations, and nodal normal displacements of the free boundaries;

(ii) displacement of the free boundaries according to the results obtained in (i), and relocation of the interface nodes on their constraining loci;

(iii) mesh conditioning;

(iv) correction of the velocity and pressure nodal values from the results obtained in (i), (ii), and (iii), in order to take into account the change of mesh topology.

*Linearisation of the Continuous Weak Equations*

The linear equation to be obtained in the continuous case has the form

$$\langle H(X_m)\,\bar{\delta}X_m,\,\delta Y\rangle + \langle G(X_m),\,\delta Y\rangle = 0, \qquad \forall\,\delta Y \in \Xi(X_m). \tag{68}$$

It requires computing the variation of (21) including variations of the domain of integration. Examples of the use of such variations may be found in the papers by Luke [23], Ikegawa and Washizu [24], and Dupret [8], for solving inviscid flow problems, and in Dupret [9], for solving viscous flow problems. The theory is developed in Dupret [7, 8].

Let $\Omega^{\Pi}$ denote a family of flow domains which continuously depend on one or several parameters ($\Pi$). The boundary $\partial\Omega^{\Pi}$ consists of a free part $\partial\Omega_f^{\Pi}$, of extremities $R^{\Pi}$ and $S^{\Pi}$, and an unvarying part $\partial\Omega_u^{\Pi}$. Symbols $\mathbf{n}$, $\mathbf{s}$, $s$, $\theta$, and $\phi$ have the same meaning as in Subsections 2.1 and 2.2. For any infinitesimal variation $\bar{\delta}\Pi$ of the parameters, $\bar{\delta}\alpha(s)$ stands for the first-order terms of the distance between $\partial\Omega_f^{\Pi}$ and $\partial\Omega_f^{\Pi+\bar{\delta}\Pi}$, as measured along the normal $\mathbf{n}^{\Pi}(s)$, while $\bar{\delta}\gamma(R^{\Pi})$ and $\bar{\delta}\gamma(S^{\Pi})$ are the first-order terms of the displacements of the extremities $R^{\Pi}$ and $S^{\Pi}$, measured along the tangents $\mathbf{s}_u(R^{\Pi})$ and $\mathbf{s}_u(S^{\Pi})$ to $\partial\Omega_u^{\Pi}$ (Fig. 11).

Consider any scalar field $f^{\Pi}(\mathbf{x})$, which is defined on $\Omega^{\Pi}$ and continuously depends on $\Pi$. Let $\bar{\delta}f(\mathbf{x})$ denote the first variation of $f^{\Pi}$, i.e., the first-order terms in the expansion of $(f^{\Pi+\bar{\delta}\Pi}(\mathbf{x}) - f^{\Pi}(\mathbf{x}))$ in powers of $\bar{\delta}\Pi$ (observe that both $f^{\Pi+\bar{\delta}\Pi}$ and $f^{\Pi}$ are evaluated at the same location $\mathbf{x}$). In a similar manner, let $\mathbf{v}^{\Pi}(\mathbf{x})$ and $\bar{\delta}\mathbf{v}(\mathbf{x})$ stand for any vector field and its first variation. The following theorems allow us to calculate the first variation of functionals defined from $f^{\Pi}(\mathbf{x})$ or $\mathbf{v}^{\Pi}(\mathbf{x})$:

$$\bar{\delta}\int_{\Omega^{\Pi}} f^{\Pi}\,d\sigma = \int_{\Omega^{\Pi}} \bar{\delta}f\,d\sigma + \int_{\partial\Omega_f^{\Pi}} f^{\Pi}\,\bar{\delta}\alpha\,ds; \tag{69}$$

$$\bar{\delta}\int_{\partial\Omega_f^{\Pi}} f^{\Pi}\,ds = \int_{\partial\Omega_f^{\Pi}} \left[\bar{\delta}f + \frac{\partial f^{\Pi}}{\partial n}\,\bar{\delta}\alpha - \phi\,\frac{\partial(f^{\Pi}\,\bar{\delta}\alpha)}{\partial s}\right] ds + [f^{\Pi}(\phi\,\bar{\delta}\alpha - \cos\theta\,\bar{\delta}\gamma)]_{\partial\Omega_f^{\Pi}}; \tag{70}$$

$$\bar{\delta}\int_{\partial\Omega_u^{\Pi}} f^{\Pi}\,ds = \int_{\partial\Omega_u^{\Pi}} \bar{\delta}f\,ds + [f^{\Pi}\,\bar{\delta}\gamma]_{\partial\Omega_u^{\Pi}}; \tag{71}$$

$$\bar{\delta}\int_{\partial\Omega_f^{\Pi}} \mathbf{v}^{\Pi}\cdot\mathbf{n}\,ds = \int_{\partial\Omega_f^{\Pi}} [\bar{\delta}\mathbf{v}\cdot\mathbf{n} + \nabla\cdot\mathbf{v}\,\bar{\delta}\alpha]\,ds + [\mathbf{v}^{\Pi}\times\mathbf{s}_u\,\bar{\delta}\gamma]_{\partial\Omega_f^{\Pi}}. \tag{72}$$

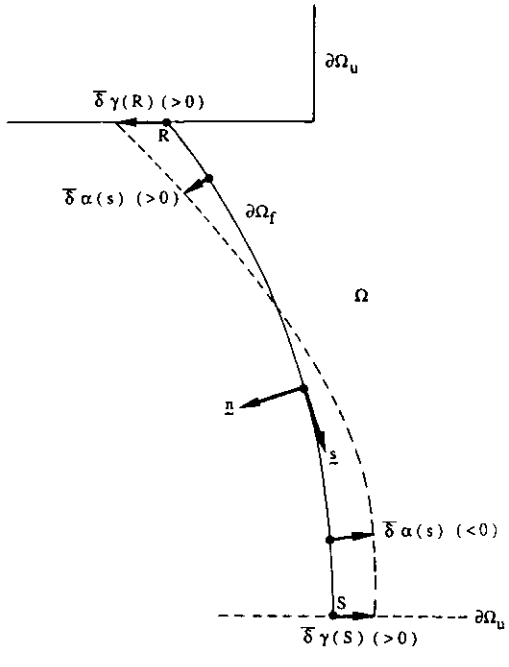


**FIG. 11.** Free surface iterative displacement; definition of $\bar{\delta}\alpha(s)$, $\bar{\delta}\gamma(R)$, and $\bar{\delta}\gamma(S)$.

The validity of these formulae is, of course, subject to some constraints on the regularity of $\Omega^{\Pi}$, and of $f^{\Pi}(\mathbf{x})$ or $\mathbf{v}^{\Pi}(\mathbf{x})$. In particular, defining appropriate extensions of the latter functions over $\Omega^{\Pi} \cup \Omega^{\Pi+\delta\Pi}$ must be possible. Some aspects of these difficult questions are addressed in Dupret [7].

If the continuous case expansion (68) is desired, it seems to be sufficient to take the first variation $\bar{\delta}(\delta M)$, which yields $H(X)$ from

$$\langle H(X)\,\bar{\delta}X, \delta Y\rangle = \bar{\delta}(\delta M). \tag{73}$$

However, a first problem lies in defining $(X+\bar{\delta}X)$ from $X$ and $\bar{\delta}X$, since the latter belongs to the tangent linear space $\Xi(X)$, while $X$ and $(X+\bar{\delta}X)$ both belong to the nonlinear space $\Psi$. Moreover, in contrast with the case of a problem in a fixed domain, fixing the test function $\delta Y$ when expanding $\delta M$ in powers of $\bar{\delta}X$ becomes meaningless, since $\delta Y$ belongs to the space $\Xi(X)$, which depends on $X$. The solution consists in projecting the spaces $\Xi(X+\bar{\delta}X)$ onto $\Xi(X)$ in some vicinity of $X$. The expression $\bar{\delta}(\delta M)$ is then obtained by expanding $\delta M(X+\bar{\delta}X)$ while fixing the projection of $\delta Y$ onto $\Xi(X)$.

The particular method which we use for solving free boundary problems is the following:

(i) the first variations $\bar{\delta}\mathbf{v}(\mathbf{x})$ and $\bar{\delta}p(\mathbf{x})$ of the velocity and pressure fields are defined on fixed points of the flow domain $\bigcup_i \Omega^{(i)}$ as explained above;

(ii) any Lagrange multiplier $\lambda(s)$ is extended in the vicinity of its definition interface $\partial\Omega_f^{(i)}$ by assuming that the extended function is constant on any normal to $\partial\Omega_f^{(i)}$:

$$\frac{\partial\lambda}{\partial n} = 0; \tag{74}$$

hence, the first variation $\bar{\delta}\lambda(s)$ may be defined as in (i);

(iii) the first variation $\bar{\delta}\alpha(s)$ is measured along the normals to the interfaces, as explained above;

(iv) the projections of the test functions $\delta\mathbf{v}(\mathbf{x})$ and $\delta p(\mathbf{x})$ from $\Xi(X+\bar{\delta}X)$ onto $\Xi(X)$ are defined as being the same functions, except that their domain becomes $\bigcup_i \Omega^{(i)}$, with appropriate extensions if necessary; this means that we may formally write:

$$\begin{aligned} &\bar{\delta}(\delta\mathbf{v})(\mathbf{x}) = \mathbf{0}, \\ &\bar{\delta}(\delta p)(\mathbf{x}) = 0, \qquad \mathbf{x} \in \bigcup_i \Omega^{(i)}; \end{aligned} \tag{75}$$

(v) any test Lagrange multiplier $\delta\lambda(s)$ (and, in particular, $\delta\alpha(s)$) is extended as explained in (ii); projections are defined in such a manner that the following relations hold on the interface:

$$\begin{aligned} &\bar{\delta}(\delta\lambda)(s) = 0, \\ &\bar{\delta}(\delta\alpha)(s) = 0, \qquad \mathbf{x} \in \partial\Omega_f^{(i)}; \end{aligned} \tag{76}$$

(vi) any arbitrary test number $\delta K$ is kept constant when projected onto $\Xi(X)$; hence, we write

$$\bar{\delta}(\delta K) = 0. \tag{77}$$

On this basis, the complete development of $\bar{\delta}(\delta M)$ may be calculated. The result is given in the Appendix. The linear system to be solved at each iteration is obtained from the continuous form (68) by using the approximations (47) to (49). The solution is found by applying the minimum degree ordering (MDO) algorithm (see George and Liu [25]), in a version adapted to solving non-symmetric systems (Berghezan [26]).

It should be observed that obtaining the expansion (68) from (73) required to express all the conditions holding on the interfaces, and the variable inlet and outlet sections, in a weak form (by means of Lagrange multipliers). Indeed, the first variation $\bar{\delta}(\delta M)$ could not be obtained easily if the unknown fields were constrained by essential conditions on the free boundaries. On the other hand, the necessity of using a priori discontinuous velocity fields (the continuity being weakly imposed) is obvious when considering that first variations $\bar{\delta}\mathbf{v}(\mathbf{x})$ are normally discontinuous on the interfaces, as being calculated on fixed points of the flow domain.

*Global Iterative Algorithm*

From the nodal normal displacements $\bar{\delta}\alpha_r$, together with the extremity displacements $\bar{\delta}\gamma(R)$ and $\bar{\delta}\gamma(S)$, the new configuration of any interface is easily calculated. New interface nodes $\mathbf{x}_r$ are relocated on their constraining loci and the mesh conditioning procedure provides new locations of the internal nodes. As incremental nodal values $\bar{\delta}\mathbf{v}_k$, $\bar{\delta}p_m$, and $\bar{\delta}\lambda_q$ are defined on old nodes, computation of the new nodal values of the unknowns is performed in two steps. First, provisional values are calculated at old nodes by

$$\mathbf{v}_k^* = \mathbf{v}_k^{(\text{old})} + \bar{\delta}\mathbf{v}_k, \tag{78}$$

and similarly for $p_m^*$ and $\lambda_q^*$. Then, nodal values are corrected from

$$\begin{aligned} \mathbf{v}_k^{(\text{new})} = \mathbf{v}_k^* &+ \tfrac{1}{2}(\mathbf{x}_k^{(\text{new})} - \mathbf{x}_k^{(\text{old})}) \\ &\cdot (\nabla\mathbf{v}_k^{(\text{new})} + \nabla\mathbf{v}_k^*), \end{aligned} \tag{79}$$

and the same for $p_m^{(\text{new})}$ and $\lambda_q^{(\text{new})}$. Details are given in Dupret [8]. It is worth mentioning that solving the coupled linear system, at each iteration, is far more expensive than performing all the remaining operations.

In its original form, this global iterative scheme has shown to fail in some cases as a consequence either of too high increments, especially during the first iterations, or of divergence of the mesh conditioning procedure. In order to nonetheless obtain convergence in these situations, the following method has been used:

(i) when any nodal increment is higher than a prescribed norm, a common underrelaxation factor is applied to all increments in order to lower the critical value below the pre-selected level (using this technique concerns only a few iterations of the scheme and does not affect the subsequent quasi-quadratic convergence rate);

(ii) when necessary, the interface displacement—mesh conditioning—nodal correction procedure is performed in several subcycles, without significant increase of the global cost.

The solution procedure presented here—as based on a variational approach—is an interesting alternative to the more classical use of an exact Newton method for solving free surface problems. Although the theory is quite complex, an important advantage is that the Jacobian (or stiffness) matrix is not dependent on the particular mesh correction technique. Solving the linear systems and moving the mesh are decoupled operations, whence the radius of convergence of the iterative scheme seems to be enlarged (because the strong non-linearity of the mesh conditioning procedure has no influence on the global convergence rate). A detailed discussion may be found in Cuvelier and Schulkes [27]. Another advantage is that developing the stiffness matrix for the continuous problem before building the discrete equations facilitates any change of discretisation, such as a change of degree of the polynomial approximants (this technique has been used in Levieux *et al.* [17]). Examples are analysed in the next section.

## 4. RESULTS AND DISCUSSION

As announced in Section 1, we analyse here (a) the outflow from a planar slot and (b) the curtain flow (Fig. 1). In both cases, parametric studies are performed around a basic solution in order to determine the sensitivity of the result with respect to the material and flow parameters.

Three liquid layers are considered. Viscosities, interface tensions, contact angles, and flow rates are given in Table I for the basic problem, whose solution is shown in Figs. 12 and 13. The quality of these results is obvious. Interfaces, streamlines, and velocity isolines are smooth, while strongly distorted elements are absent in the deformed mesh. In both cases, the solution exhibits the expected physical behaviour, and, in particular, the flow domain appears to be the location of an important—upstream to downstream—reorganization of developed flows. Indeed,

**TABLE I**

Data for the Basic Problem

| | |
|---|---|
| Specific mass of each liquid | 1 g/cm$^3$ |
| Dynamic viscosity | |
| layer (1) | 15 mPa s |
| layer (2) | 30 mPa s |
| layer (3) | 5 mPa s |
| Flow rate of each liquid layer | 1 l/m/min |
| Liquid–atmosphere interface tension | 40 mN/m |
| Liquid–liquid interface tension | 0 |
| Contact angle between wall and rear curtain layer | 70° |

the shear influence of a fixed wall, from which a new (a) fluid–fluid or (b) fluid–atmosphere interface separates, suddenly ceases. However, related to the elliptic character of the Navier–Stokes equations, streamline reorganization starts upstream of the separation line.

The first parametric study is performed by letting the flow rate of the lower fluid layer vary in case (a). The successive interfaces between this layer and the adjacent upper one are shown in Fig. 14. We observe that, at low flow rates, the separation line is located under the salient corner, whose attractive influence is obvious. At higher flow rates, the line separates from this corner. No solution has been obtained with a separation line located above the corner. As fluid–fluid interface tension vanishes, it must be kept in mind that location of the separation line cannot be imposed in the analytical solution. However, imposing this location is allowed (and necessary) in numerical calculations when the distance between the separation line and the salient corner is much lower than the characteristic size of the surrounding mesh. In this case, numerical calculations are not able to tell whether the distance is—or is not—vanishing. Only more refined meshes could give a more precise answer.

The second set of solutions (Fig. 15) illustrates the situation with a separation line located above the salient corner. Both a high flow rate of the lower fluid layer and a non-vanishing fluid–fluid interface tension were necessary to obtain these results. When the interface tension tends to zero, with a fixed imposed contact angle, the location of the separation line tends towards the corner. Hence, the previous conclusion, emphasizing the strong attractive influence of this corner, is enforced.

The third and fourth parametric studies are devoted to analysing in case (b) the influence of the separation contact angle and the flow rate of the rear layer, respectively (Figs. 16 and 17). It may be observed that both the location of the separation line and the asymptotic location of the curtain are very sensitive to the flow parameters. More stable solutions would be obtained by designing a sharper coating device extremity. The upstream behaviour of the forward fluid–atmosphere interface is also noteworthy. The strongly damped oscillations of this interface are related to the presence of steady capillary waves.

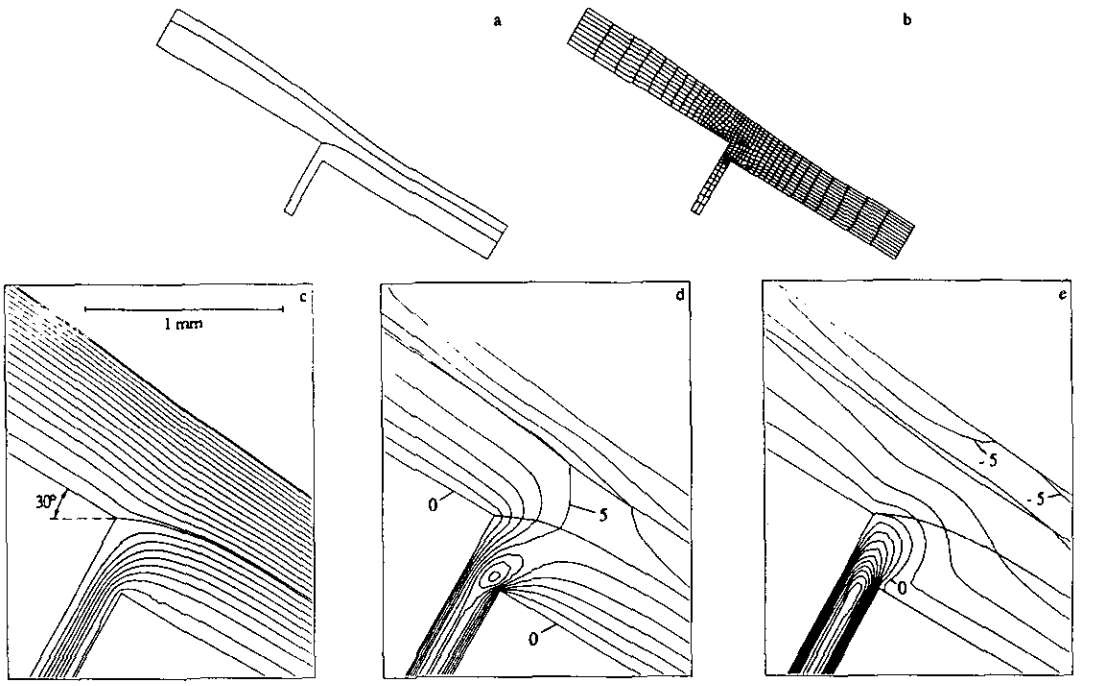


FIG. 12. Outflow from a planar slot: a. calculated interfaces; b. converged mesh; c. streamlines; d, e. isolines of horizontal and vertical velocity components by steps of 1 cm/s.

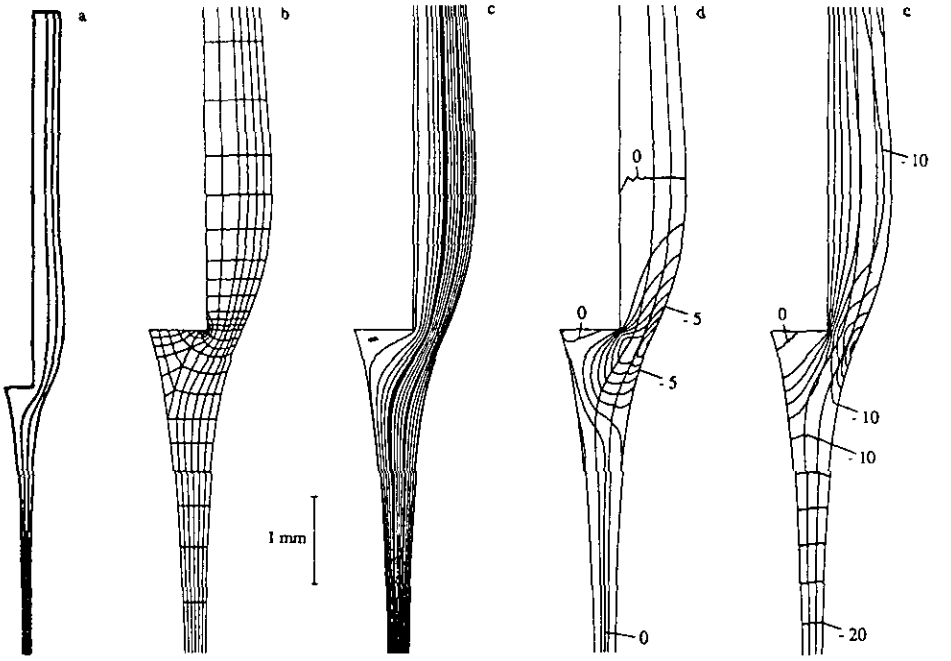


FIG. 13. Curtain flow: a. calculated interfaces; b. converged mesh; c. streamlines; d. isolines of horizontal velocity component by steps of 1 cm/s; e. isolines of vertical velocity component by steps of 2 cm/s.

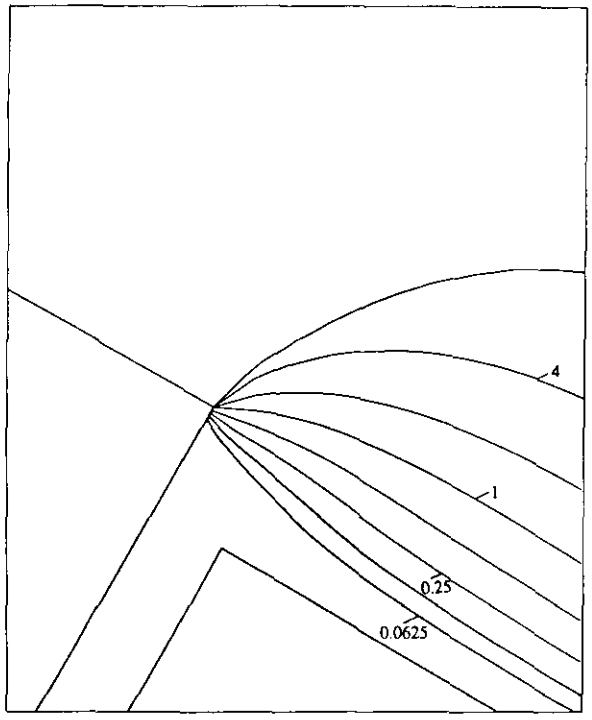


FIG. 14. Outflow from a planar slot; influence of increasing the lower flow rate (in l/m/min) on the lower interface.

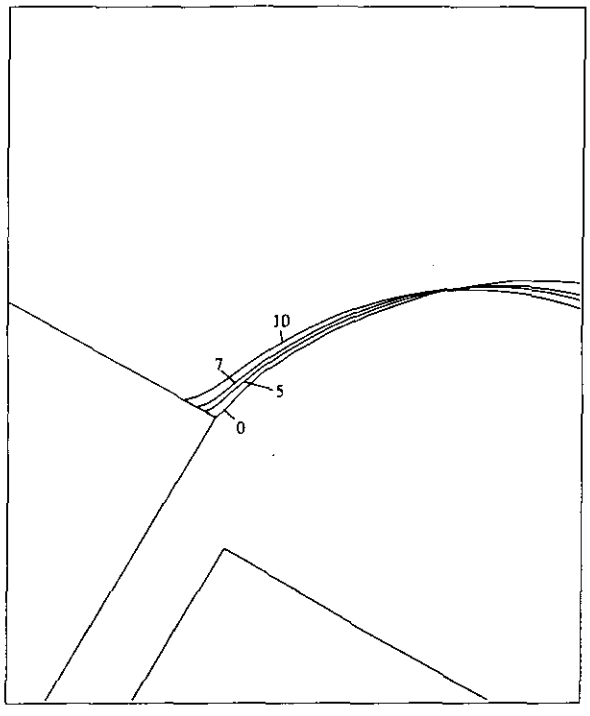


FIG. 15. Outflow from a planar slot; influence of decreasing the lower interface tension (in mN/m) on the lower interface. The lower flow rate is 8 l/m/min and the contact angle is 40°.

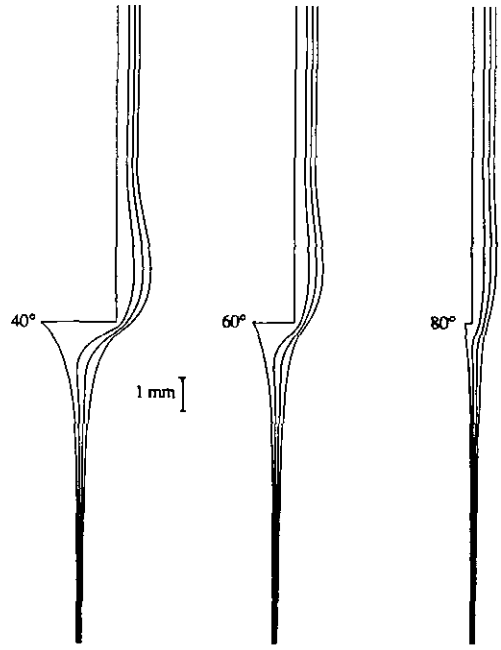


FIG. 16. *Curtain flow: influence of increasing the contact angle.*

Obtaining the solution was easy, or more or less difficult, depending on the case. A quasi-quadratic convergence of the iterative scheme is generally observed, but only in the vicinity of the solution. Finding a first solution is always harder than performing a parametric study, and case (b) is much more difficult to handle than case (a).

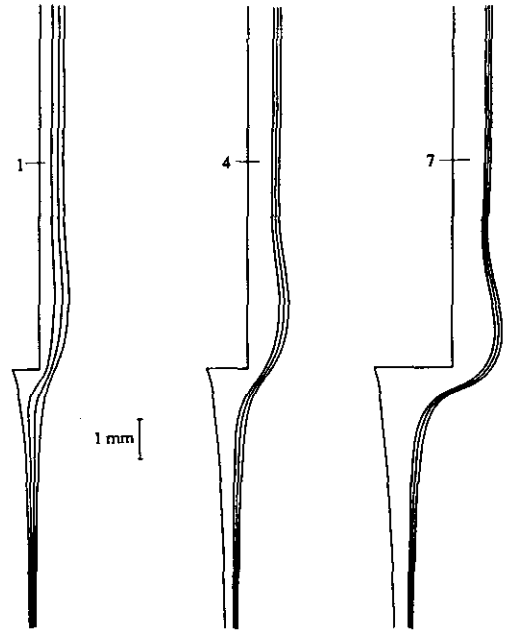


FIG. 17. Curtain flow: influence of increasing the flow rate (in l/m/min) of the rear layer.

Some particular techniques were useful in facilitating the obtention of the first solution, essentially in case (b):

— starting from smooth initial interfaces and exact asymptotic layer thicknesses;

— introducing high artificial fluid–fluid and fluid–atmosphere interface tensions (typically, 50 mN/m); the correct result is obtained by performing a parametric decrease towards the actual values;

— alternating blocked and free iterations, which means that after each full iteration, interfaces are fixed and a solution is found which does not satisfy the normal force interface conditions;

— using the underrelaxation method described in Subsection 3.3 (typically, normal displacement of free boundary nodes is limited to $10^{-2}$ cm);

— sub-cycling the displacement and correction procedure, as explained in Subsection 3.3 (typically, when the normal displacement is of the same order of magnitude as $10^{-2}$ cm, three sub-cycles are used).

## 5. CONCLUSIONS

We have presented a variational method for solving the Newtonian steady state flows involved in the coating process. Application of this method to simulating the outflow from a slot and the curtain flow has shown good results. Further work will deal with flow stability analysis.

## APPENDIX: LINEARIZATION OF THE SYSTEM

Linearization of the continuous form (21) is performed by applying the theory presented in Subsection 3.3. Following Dupret [7, 8], Eq. (20) may be introduced into the result in order to simplify the linear system. Shortened notations (28), (39), and

$$\begin{aligned} &\bar\delta\,\delta fg = \bar\delta f\,\delta g + \delta f\,\bar\delta g, \\ &\bar\delta\,\delta f^2 = 2\,\bar\delta f\,\delta f \end{aligned} \tag{A1}$$

are used. After calculation, variational formulae (69) to (72) and (74) to (77) yield

$$\begin{aligned} \bar\delta\,\delta M_1 = \sum_i \int_{\Omega^{(i)}} &[\rho^{(i)}\,\bar\delta(\mathbf{v}\cdot\nabla\mathbf{v})\cdot\delta\mathbf{v} \\ &+ \mu^{(i)}\,\bar\delta\,\delta(\mathbf{D}:\mathbf{D}) - \bar\delta\,\delta(p\nabla\cdot\mathbf{v})]\,d\sigma \\ &+ \sum_{\substack{i=0 \text{ or } N \\ (\partial\Omega_f^{(i)} \text{ free})}} \int_{\partial\Omega_f^{(i)}} [\rho^{(i)}\mathbf{v}\cdot\nabla\mathbf{v}\cdot\delta\mathbf{v} \\ &+ 2\mu^{(i)}\,\mathbf{D}:\delta\mathbf{D} - \delta(p\nabla\cdot\mathbf{v})]\,\bar\delta\alpha\,ds \\ &+ \sum_{i\neq 0,N} \int_{\partial\Omega_f^{(i)}} [\rho^{(i)}\mathbf{v}^{(i)}\cdot\nabla\mathbf{v}^{(i)}\cdot\delta\mathbf{v}^{(i)} \\ &- \rho^{(i+1)}\mathbf{v}^{(i+1)}\cdot\nabla\mathbf{v}^{(i+1)}\cdot\delta\mathbf{v}^{(i+1)} \\ &+ 2\mu^{(i)}\,\mathbf{D}^{(i)}:\delta\mathbf{D}^{(i)} - 2\mu^{(i+1)}\,\mathbf{D}^{(i+1)}:\delta\mathbf{D}^{(i+1)} \\ &- \delta(p^{(i)}\nabla\cdot\mathbf{v}^{(i)}) + \delta(p^{(i+1)}\nabla\cdot\mathbf{v}^{(i+1)})]\,\bar\delta\alpha\,ds, \end{aligned} \tag{A2}$$

$$\begin{aligned} \bar\delta\,\delta M_2^f = -\sum_{\substack{i=0 \text{ or } N \\ (\partial\Omega_f^{(i)} \text{ free})}} \Big\{ &\int_{\partial\Omega_f^{(i)}} [\bar\delta\,\delta(\lambda_n v_n) \\ &+ \delta(\nabla\cdot(\lambda_n\mathbf{v}))\,\bar\delta\alpha]\,ds \\ &- [\delta(\lambda_n v_n)\cos\theta\,\bar\delta\gamma + \delta(\lambda_n v_s)\,\bar\delta\alpha]_{\partial\Omega_f^{(i)}} \Big\} \\ - \sum_{i\neq 0,N} \Big\{ &\int_{\partial\Omega_f^{(i)}} [\bar\delta\,\delta(\lambda_n^- v_n^{(i)} - \lambda_n^+ v_n^{(i+1)}) \\ &+ \delta(\nabla\cdot(\lambda_n^-\mathbf{v}^{(i)} - \lambda_n^+\mathbf{v}^{(i+1)}))\,\bar\delta\alpha]\,ds \\ &- [\delta(\lambda_n^- v_n^{(i)} - \lambda_n^+ v_n^{(i+1)})\cos\theta\,\bar\delta\gamma \\ &+ \delta(\lambda_n^- v_s^{(i)} - \lambda_n^+ v_s^{(i+1)})\,\bar\delta\alpha]_{\partial\Omega_f^{(i)}} \Big\} \\ - \sum_{i\neq 0,N} \Big\{ &\int_{\partial\Omega_f^{(i)}} [\bar\delta\,\delta(\lambda_s(v_s^{(i)} - v_s^{(i+1)})) \\ &+ \delta(\nabla\times(\lambda_s(\mathbf{v}^{(i)} - \mathbf{v}^{(i+1)})))\,\bar\delta\alpha]\,ds \\ &- [\delta(\lambda_s(v_s^{(i)} - v_s^{(i+1)}))\cos\theta\,\bar\delta\gamma \\ &- \delta(\lambda_s(v_n^{(i)} - v_n^{(i+1)}))\,\bar\delta\alpha]_{\partial\Omega_f^{(i)}} \Big\}, \end{aligned} \tag{A3}$$

$$\begin{aligned} \bar\delta\,\delta M_2^e = -\sum_{\substack{i=1 \\ (\partial\Omega_e^{(i)} \text{ free})}}^{N} \Big\{ &\int_{\partial\Omega_e^{(i)}} \bar\delta\,\delta(c^{(i)}v_n + \lambda_s v_s)\,ds \\ &+ [\delta(c^{(i)}v_n + \lambda_s v_s)\,\bar\delta\gamma]_{\partial\Omega_e^{(i)}} \Big\}, \end{aligned} \tag{A4}$$

$$\begin{aligned} \bar\delta\,\delta M_2^o = -\sum_{i=1}^{N} \Big\{ &\int_{\partial\Omega_o^{(i)}} [\bar\delta k^{(i)}\,\delta v_n + \bar\delta\,\delta(\lambda_s v_s)]\,ds \\ &+ [(k^{(i)}\,\delta v_n + \delta(\lambda_s v_s))\,\bar\delta\gamma]_{\partial\Omega_o^{(i)}} \Big\} \\ &+ \sum_{i=1}^{N-1} (\bar\delta(k^{(i)} - k^{(i+1)}) \\ &+ \nabla(V^{(i)} - V^{(i+1)})\cdot\mathbf{s}\,\bar\delta\gamma)_{S^i}\,\delta k^{(i)} \\ &+ (\bar\delta k^{(N)} + \nabla V^{(N)}\cdot\mathbf{s}\,\bar\delta\gamma)_{S^N}\,\delta k^{(N)}, \end{aligned} \tag{A5}$$

$$\bar{\delta}\,\delta M_3^{\lambda} = -\sum_{\substack{i=0 \text{ or } N \\ (\partial\Omega_f^{(i)} \text{ free})}} \left\{ \int_{\partial\Omega_f^{(i)}} \left[ \bar{\delta}\lambda_n\,\delta\alpha + \frac{1}{2}\frac{\partial V^{(i)}}{\partial n}\,\bar{\delta}\,\delta\alpha^2 - \frac{1}{2}\phi\frac{\partial}{\partial s}\left((\lambda_n + V^{(i)})\,\bar{\delta}\,\delta\alpha^2\right)\right] ds - \left[\frac{1}{2}(\lambda_n + V^{(i)})(\cos\theta\,\bar{\delta}\,\delta\alpha\gamma - \phi\,\bar{\delta}\,\delta\alpha^2)\right]_{\partial\Omega_f^{(i)}} \right\}$$

$$- \sum_{i\neq 0,N} \left\{ \int_{\partial\Omega_f^{(i)}} \left[ \bar{\delta}(\lambda_n^- - \lambda_n^+)\,\delta\alpha + \frac{1}{2}\frac{\partial}{\partial n}(V^{(i)} - V^{(i+1)})\,\bar{\delta}\,\delta\alpha^2 - \frac{1}{2}\phi\frac{\partial}{\partial s}\left((\lambda_n^- - \lambda_n^+ + V^{(i)} - V^{(i+1)})\,\bar{\delta}\,\delta\alpha^2\right)\right] ds - \left[\frac{1}{2}(\lambda_n^- - \lambda_n^+ + V^{(i)} - V^{(i+1)}) \times (\cos\theta\,\bar{\delta}\,\delta\alpha\gamma - \phi\,\bar{\delta}\,\delta\alpha^2)\right]_{\partial\Omega_f^{(i)}} \right\}, \tag{A6}$$

and

$$\bar{\delta}\,\delta M_3^{\sigma} + \bar{\delta}\,\delta M_3^{\gamma} = -\sum_{\substack{i \\ (\partial\Omega_f^{(i)} \text{ free})}} \left\{ \int_{\partial\Omega_f^{(i)}} \sigma^{(i)} \frac{d\,\delta\alpha}{ds}\frac{d\,\bar{\delta}\alpha}{ds}\,ds + \left[\frac{1}{2}\sigma^{(i)}\chi_w\,\bar{\delta}\,\delta\alpha\gamma\right]_{\partial\Omega_f^{(i)}} \right\}, \tag{A7}$$

where the symbol $\chi_w$ denotes the curvature of the wall.

It is convenient to introduce additional Lagrange multipliers $\zeta(R_i)$ and $\zeta(S_i)$ at the ends of the free boundaries and to define the forms

$$\delta L = \sum_{\substack{i \\ (\partial\Omega_f^{(i)} \text{ free})}} \left[-\zeta\,\delta\alpha + \zeta\,\delta\gamma\sin\theta\right]_{\partial\Omega_f^{(i)}} \tag{A8}$$

and

$$\bar{\delta}\,\delta L = \sum_{\substack{i \\ (\partial\Omega_f^{(i)} \text{ free})}} \left[-\bar{\delta}\,\delta\alpha\zeta + \bar{\delta}\,\delta(\gamma\zeta)\sin\theta\right]_{\partial\Omega_f^{(i)}}, \tag{A9}$$

which are added to $\delta M$ and $\bar{\delta}\,\delta M$, as defined by (21), (25), and (73). Symbols $\delta\zeta(R_i)$ and $\delta\zeta(S_i)$ are arbitrary numbers which, from (A9), impose that

$$\delta\gamma = \bar{\delta}\alpha/\sin\theta, \qquad \text{at } R_i \text{ or } S_i, \tag{A10}$$

be satisfied. Symbols $\delta\gamma(R_i)$ and $\delta\gamma(S_i)$ are no longer related to $\delta\alpha(R_i)$ and $\delta\alpha(S_i)$ by Eq. (44), so they become arbitrary numbers. The weak formulation is, however, equivalent.

## ACKNOWLEDGMENTS

Financial support for this work was provided by Agfa-Gevaert Company. The authors wish to thank B. Goetmaeckers, J. Hens, and W. Van Abbenyen for many valuable discussions.

## REFERENCES

1. W. Pulkrabek and R. Wabrek, in *AIChE Int. Symp. on Mech. Thin-Film Coating, New Orleans, March 6–10, 1988*, Paper 4A.
2. B. M. Deryagin and S. M. Levi, *Film Coating Theory* (Focal Press, London/New York, 1964).
3. H. Saito and L. E. Scriven, *J. Comput. Phys.* **42**, 53 (1981).
4. S. F. Kistler and L. E. Scriven, in *Computational Analysis of Polymer Processing*, edited by J. R. A. Pearson and S. M. Richardson (Appl. Sci., Braking, Essex, UK, 1983), p. 243.
5. S. F. Kistler, Ph.D. thesis, University of Minnesota, Minneapolis, 1984 (unpublished).
6. K. N. Christodoulou and L. E. Scriven, *J. Sci. Comput.* **3**, 355 (1988).
7. F. Dupret, Ph.D. thesis, Université Catholique de Louvain, Louvain-la-Neuve, 1981 (unpublished).
8. F. Dupret, *J. Mec.* **20**, 659 (1981).
9. F. Dupret, in *Finite Element Flow Analysis*, edited by T. Kawai (University of Tokyo Press, Tokyo, 1982).
10. I. Babuška, *Numer. Math.* **20**, 179 (1973).
11. K. J. Ruschak, *Int. J. Numer. Methods Eng.* **15**, 639 (1980).
12. N. P. Kruyt, C. Cuvelier, A. Segal, and J. Van Der Zanden, *Int. J. Numer. Methods Fluids* **8**, 351 (1988).
13. N. S. Clarke, *J. Fluid Mech.* **31**, 481 (1968).
14. H. K. Moffat, *J. Fluid Mech.* **18**, 1 (1964).
15. D. Scanlan and L. E. Scriven, in *AIChE Int. Symp. on Mech. Thin-Film Coating, Orlando, March 18–22, 1990*, Paper 35E.
16. D. H. Michael, *Mathematika* **5**, 82 (1958).
17. F. Levieux, D. Berghezan, and F. Dupret, in *Proceedings ICOSAHOM'92*; *Comput. Methods Appl. Mech. Eng.* **115**, to appear.
18. G. Strang and G. J. Fix, *An Analysis of the Finite Element Method* (Prentice-Hall, Englewood Cliffs, NJ, 1973).
19. O. C. Zienkiewicz, *The Finite Element Method*, 3rd ed. (McGraw-Hill, London, 1977).
20. J. Dheur and M. J. Crochet, *Rheol. Acta* **26**, 401 (1987).
21. R. E. Nickell, R. I. Tanner, and B. Caswell, *J. Fluid Mech.* **65**, 189 (1974).
22. W. J. Silliman and L. E. Scriven, *J. Comput. Phys.* **34**, 287 (1980).
23. J. C. Luke, *J. Fluid Mech.* **27**, 395 (1967).
24. M. Ikegawa and K. Washizu, *Int. J. Numer. Methods Eng.* **6**, 179 (1973).
25. A. George and J. W. Liu, *Computer Solution of Large Sparse Positive Definite Systems*, Series in Computational Mathematics (Prentice-Hall, Englewood Cliffs, NJ, 1981).
26. D. Berghezan, Ph.D. thesis, Université Catholique de Louvain, Louvain-la-Neuve, 1991 (unpublished).
27. C. Cuvelier and R. M. S. M. Schulkes, *SIAM Rev.* **32**, 355 (1990).